How to cite: *Angew. Chem. Int. Ed.* **2020**, *59*, 13238–13245
International Edition: doi.org/10.1002/anie.202002180
German Edition: doi.org/10.1002/ange.202002180

VIP **Self-Assembly** *Very Important Paper*

Transient DNA-Based Nanostructures Controlled by Redox Inputs

*Erica Del Grosso, Leonard J. Prins, and Francesco Ricci**

Abstract: *Synthetic DNA has emerged as a powerful self-assembled material for the engineering of nanoscale supramolecular devices and materials. Recently dissipative self-assembly of DNA-based supramolecular structures has emerged as a novel approach providing access to a new class of kinetically controlled DNA materials with unprecedented life-like properties. So far, dissipative control has been achieved using DNA-recognizing enzymes as energy dissipating units. Although highly efficient, enzymes pose limits in terms of long-term stability and inhibition of enzyme activity by waste products. Herein, we provide the first example of kinetically controlled DNA nanostructures in which energy dissipation is achieved through a non-enzymatic chemical reaction. More specifically, inspired by redox signalling, we employ redox cycles of disulfide-bond formation/breakage to kinetically control the assembly and disassembly of tubular DNA nanostructures in a highly controllable and reversible fashion.*

Introduction

Supramolecular materials have emerged as a class of materials with unique properties.[1–11] Owing to the non-covalent interactions between the monomers, these materials self-assemble spontaneously and are dynamic in nature. As a result, the materials' properties are a function of the physicochemical environment, which allows the adaptation to chemical or physical inputs.[1,4,12,13] These materials are generally at thermodynamic equilibrium, which implies that the responsiveness is determined by the change in the free energy landscape induced by the external stimulus. The clear advantage of operating at thermodynamic equilibrium is the intrinsic long-term stability of the material. Yet, the thermodynamically driven self-assembly approach becomes a limitation in case the functional properties of the material are required only for a limited amount of time. For these cases, nature has developed another approach in which the self-assembly of monomers is controlled by chemical fuels.[14,15] An example is the formation of microtubules, which requires complexation of GTP[14,15] by the tubulin building blocks. Hydrolysis of GTP causes destabilization and a spontaneous disassembly of the polymers. Likewise, biochemical pathways are transiently activated through the ATP-fuelled phosphorylation of proteins followed by kinase-mediated dephosphorylation.[16] The energy-dependence of self-assembly processes provides an efficient way to activate or deactivate the material and its associated properties. Implementation of dissipative self-assembly in a synthetic context provides access to a new class of materials with unprecedented life-like properties, and for this reason has attracted the interest of chemists in recent years.[17–19] This has led to the development of several chemically fuelled synthetic materials in which the functional state is controlled by the concurrent presence of an anabolic and catabolic reaction; the first one leading to the self-assembled material, the second one destroying it.[20–26]

In the past decade, synthetic DNA has emerged as a powerful self-assembly material for the engineering of nanoscale supramolecular devices and materials. The highly predictable base-pairing, the ease of synthesis, and reliability of hybridization allow synthetic nucleic acids to be conveniently used for the self-assembly of structures with quasi-Angstrom precision in the positioning of the building blocks.[27–31] Whereas the first examples of static DNA-based nanostructures relied on the folding of a long DNA strand backbone through short DNA-staples (DNA origami),[28–33] more recently a wide range of more dynamic structures have been reported in which specific chemical inputs,[34–37] or environmental triggers, such as temperature[38–40] and pH,[41–43] induce a structural reconfiguration of DNA. Yet, in all these cases adaptability originates from changes in the free energy landscape caused by the external trigger. The transient self-assembly of DNA-based nanostructures and the kinetic control of DNA-based nanodevices has only recently been achieved using synthetic gene circuits[44] or DNA-recognizing enzymes as the fuel-consuming units.[45–48] DNA self-assembly in these systems is characterized by the instalment of a dynamic kinetic steady state in which an anabolic reaction leads to DNA-hybridization, whilst a catabolic enzymatic reaction concurrently causes disassembly by hydrolysing hybridized DNA. These first examples offer a perspective on the novel properties and potential of this new class of DNA-based materials, particularly related to the possibility to regulate their lifetime in a dynamic and controlled way. These approaches exquisitely rely on the biomachinery (enzymes, in vitro transcription system, amongst others) to control the dynamic kinetic steady state. While this offers certain advantages, especially related to the high specificity of enzymatic reactions, some drawbacks might arise due to the limited stability of enzymes, the inhibition effect of waste products, and the restriction to enzyme-compatible experimental conditions. Motivated by the above arguments, here we provide the first example in which the transient self-

[*] Dr. E. Del Grosso, Prof. F. Ricci
Department of Chemistry, University of Rome
Tor Vergata, Via della Ricerca Scientifica, 00133 Rome (Italy)
E-mail: francesco.ricci@uniroma2.it
Prof. L. J. Prins
Department of Chemical Sciences, University of Padua
Via Marzolo 1, 35131 Padua (Italy)
Supporting information and the ORCID identification number(s) for the author(s) of this article can be found under: https://doi.org/10.1002/anie.202002180.

assembly of DNA-based nanostructures does not rely on enzymes or other biological systems but rather uses purely synthetic chemical reactions. More specifically, inspired by the redox signalling widely used by cells to activate or inhibit sulfur switches that act as biological sensors,[49–51] we employ here redox cycles of disulfide-bond formation/breakage to kinetically control the assembly of DNA-based nanostructures. The exploitation of redox chemistry as a new (biocompatible) control mechanism will facilitate the implementation of fuelled-DNA self-assembly processes in a synthetic context without the limitations linked to the use of enzymatic reactions.

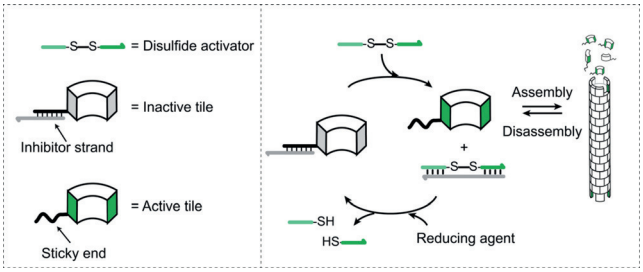

Figure 1. Transient self-assembly of DNA-based nanostructures driven by redox fuels. A disulfide activator (green) drives the transition of the DNA tiles from the inactive (grey tile) to the active form (green tile) by a strand-displacement reaction that removes an inhibitor strand from the DNA tile (right). Active tiles self-assemble into tubular structures. In the presence of a reducing agent, the disulfide activator is split into its two halves that de-hybridize from the inhibitor strand making it available for the deactivation of the tiles and nanotube disassembly.

Results and Discussion

To control in a transient way the assembly of DNA-based nanostructures using redox fuels we initially employed double-crossover DNA tiles, known as DAE-E,[52,53] that are assembled through the interaction of five different strands containing four sticky ends (each of five nucleotides; Supporting Information, Figure S1). These DNA tiles are able to self-assemble at room temperature into hollow tubular structures with a maximum observed length on the order of a few micrometres. More specifically, we used a re-engineered design[44] in which the capacity of the tiles to self-assemble at room-temperature can be easily activated or inhibited by the exogenous addition of regulator strands. Active tiles can be switched to an inactive conformation by the addition of an inhibitor strand that sequesters one of the four sticky ends and thus prevents the tiles' correct assembly (Supporting Information, Figure S2).[44] Such inactive tiles can then be re-activated by the addition of an activator strand that, through a toehold strand-displacement reaction, causes the sequestration of the inhibitor strand responsible for inactivation (Supporting Information, Figure S3).

To first demonstrate transient redox control over the assembly of such DNA structures we have split the DNA activator strand into two halves linked through a disulfide bond (Figure 1, left). The addition of this disulfide activator to a solution containing the inactivated tiles would lead to the assembly of the nanotubes (Figure 1, right). In the presence of a reducing agent the disulfide bond of the activator will be reduced allowing the two halves to be separated and thus spontaneously de-hybridize from the inhibitor (Figure 1, right). As a result, the effect of the activator will be transient and the nanotubes will gradually disassemble over time (Figure 1, right).

Instrumental for our strategy, aimed at observing the transient assembly of DNA nanostructures, is the need to find an optimal thermodynamic trade-off in which the activator should efficiently displace the inhibitor strand from the tile and, upon reduction of the disulfide bond (that leads to the separation of the activator in two halves), it should de-hybridize from the inhibitor. To achieve this, we have rationally designed disulfide activators ranging in total length from 24-nt to 8-nt (with disulfide bonds separating the activator in two halves with equal number of nucleotides; Figure 2b, see also Figure S4 in the Supporting Information for schemes of the strand-displacement reaction between activator and inhibitor). The rational behind this choice comes from previous experience with similar systems that show efficient de-hybridization with strands shorter than 10 nucleotides.[46,54] We initially tested these activator strands with a DNA control tile lacking the sticky ends and thus unable to assemble into a tubular structure. This allowed a study of the strand-displacement reaction between the activator and the inactivated tile without the complications that might arise from the self-assembly process. The tile and inhibitor were also labelled with a fluorescence optical pair (Q570 and Q670) to follow the activator-induced strand-displacement reaction (Figure 2a).

We tested the strand-displacement reaction after the addition of disulfide activators in the absence of the reducing agent. As expected, the reaction efficiency follows a length-dependent behaviour. No signal increase was observed after the addition of the shorter activators (Act_8 and Act_12) as these strands are not long enough to induce strand displacement (Figure 2c, left, and 2d). On the other hand, an efficient reaction was observed with longer activators (Act_16, Act_20, and Act_24) and the observed increase in fluorescence signal was stable, suggesting that these disulfide activators remain bound to the inhibitor over the entire course of the experiment (Figure 2c, left, and 2d). We then performed the same experiment in the presence of a reducing agent (tris(2-carboxyethyl)phosphine, TCEP; Figure 2c, right, and 2d). The behaviour of longer activators (Act_20 and Act_24) remained similar: we observed a stable signal after strand-displacement reaction. This is likely because after reduction of the disulfide bond the two activator's halves are long enough to remain stably bound to the inhibitor thus preventing its re-hybridization to the tile (Supporting Information, Figure S5). With Act_16, instead, after the fast strand-displacement reaction with the inhibitor, we observed a slower time-dependent signal decrease, which is attributed to the de-hybridization of the two reduced halves (each of 8-nt) of this activator from the inhibitor and the successive re-association of the inhibitor to the tile (Figure 2c, right, 2d, and Supporting Information, Figure S6). We note here that, when compared to a control strand with the same sequence and

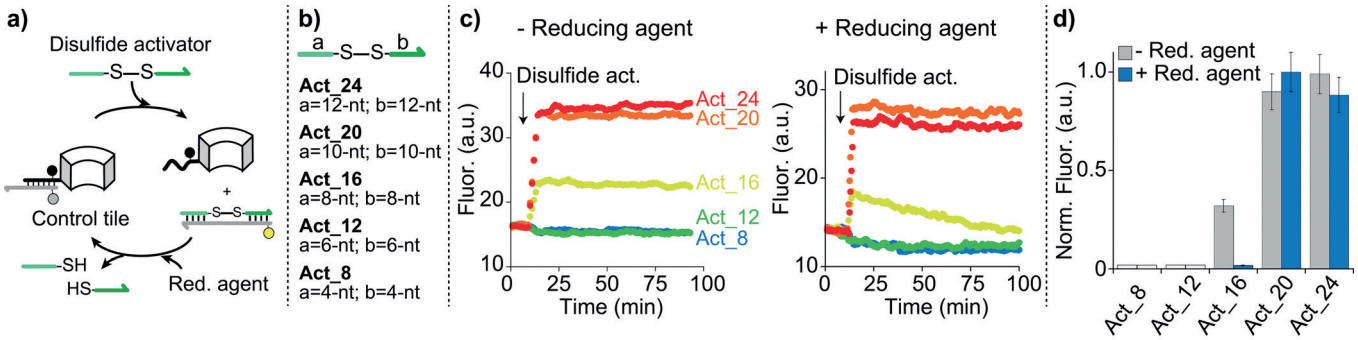

Figure 2. Transient activation of the DNA tile driven by redox fuels. a) Strand-displacement reaction between the disulfide activator and a control non-functional tile. Displacement of the inhibitor strand by the activator can be followed by fluorescence measurement. b) Disulfide activators of different lengths were employed with the disulfide bond separating the activator in two halves of identical length. The number associated to each activator's name indicates its total number of nucleotides. The number of nucleotides of the two halves is also indicated for clarity. c) Fluorescent kinetic traces of strand-displacement reactions observed by adding disulfide activators of different lengths into a solution containing the inactive non-functional tile in the absence (left) and presence (right) of a reducing agent (TCEP, 0.3 mM). d) Normalized fluorescent signals obtained from kinetic traces (end-point) in the absence (grey) and presence (blue) of the reducing agent. The strand-displacement experiments in this Figure were performed using a tile labelled with a FRET couple (Q570-Q670) so that the displacement reaction can be easily followed through increase of the fluorescence signal. Time-course experiments were performed in 1×TAE, 12.5 mM $MgCl_2$ at pH 8.0, 25 °C, DNA control tile (500 nM) in the presence and absence of TCEP (0.3 mM) used as reducing agent. The disulfide activators were added at a 3 μM concentration. In the histogram (d), the bars corresponding to "Normalized fluorescence" = 0 where no signal change is observed are shown as white bars for clarity. The experimental values represent averages of three separate measurements and the error bars reflect the standard deviations.

lacking the disulfide bond, the overall affinity of Act_16 for the tile is not affected by the presence of the disulfide bond in the middle of the strand and the strand-displacement efficiency is only partially reduced (Supporting Information, Figure S7). We have performed the same strand-displacement reaction with Act_16 using different concentrations of reducing agent. The results showed a concentration-dependent signal decay (Supporting Information, Figure S8) that further supports the hypothesis that the signal decrease observed over time is due to the de-hybridization of the reduced activator's halves from the inhibitor. This de-hybridization process might also be pushed by the presence of a 2-nt unpaired portion of the inhibitor that can initiate a strand-displacement reaction with the tile (see Figure S9 in the Supporting Information). We have also performed strand-displacement reactions in the presence of the reducing agent with control activators lacking the disulfide bond. In this case, as expected, we observed stable signals after strand-displacement reactions for all control activators longer than 16 nucleotides (Supporting Information, Figure S10).

Disulfide activators provide a means to transiently control the assembly of DNA-based nanostructures. To demonstrate this, we have tested the above-described disulfide activators in the presence of a reducing agent, but this time using inactivated tiles containing sticky-ends, which can be activated for nanostructure formation by inhibitor displacement (Figure 3a). To quantify nanotube assembly by fluorescence confocal microscopy, tiles were labelled with a fluorescent dye (Q570) by incorporating the fluorophore in one of the tile-forming DNA strands. As expected, based on the preliminary studies described above, the addition of the shorter activators (Act_8 and Act_12) did not lead to tile activation and we did not observe any nanotube structures even after 24 h from the addition of the activator. The addition of longer activators (Act_20 and Act_24), conversely, caused tile activation and

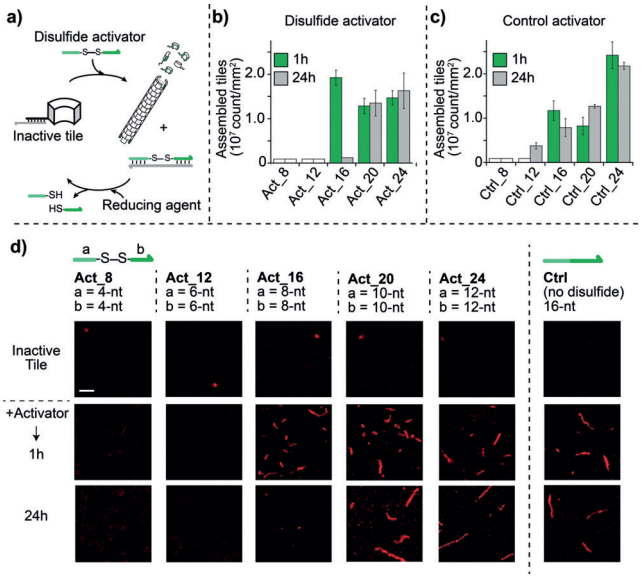

Figure 3. Transient self-assembly of DNA-based nanostructures driven by redox fuels. a) Transient self-assembly induced by a disulfide activator achieved in the presence of a reducing agent. b) Histograms of assembled tile density (assembled tile count/mm²) measured from fluorescence microscopy images taken before and after (1 h and 24 h) the addition of disulfide activators of different lengths. c) Same experiment as in (a) but using control activators lacking the disulfide bond. d) Fluorescence microscopy images obtained with the disulfide activators and one control activator (Ctrl_16). The experiments shown in this Figure were performed in 1×TAE, 12.5 mM $MgCl_2$ at pH 8.0 + TCEP (0.1 mM), 25 °C. Nanotube self-assembly was carried out in the presence of inactive DNA tiles (500 nM) by adding the disulfide or the control activator (3 μM). In the histograms (b,c), the bars corresponding to "Assembled tiles" = 0 where no nanotubes are observed are shown as white bars for a matter of clarity. The experimental values represent averages of three separate measurements and the error bars reflect the standard deviations. Scale bars for all microscopy images, 2.5 μm.

nanotube assembly. However, these nanotubes remained stable over the entire course of the experiment (namely, 24 h) likely because the reduction of the disulfide bond for such activators does not lead to the de-hybridization of the two reduced halves from the inhibitor. Only the disulfide activator with intermediate length (Act_16 with halves of 8-nt) showed transient self-assembly: micron-scale nanotubes are observed using confocal microscopy after 1 h from activator addition while no nanotubes are observed upon full reduction of the activator (after 24 h; Figure 3b–d). Of note, also in this case, control experiments using activators of the same length but lacking the disulfide bond showed that nanotubes efficiently formed with activators longer than 16 nucleotides after 1 h and remained stable over the 24 h of the experiment (Figure 3c,d, Ctrl and Supporting Information, Figure S11).

The lifetime of the nanotube assemblies can be modulated by varying the reducing strength of the solution. This could be easily achieved by changing the concentration of the reducing agent (namely, TCEP) employed during the experiment (Figure 4). As expected, in the absence of the reducing agent, the addition of the disulfide activator (Act_16) resulted in the formation of stable nanotube structures (Figure 4b, blue and Figure 4c). By gradually increasing the TCEP concentration in the solution, transient self-assembly was observed with a [TCEP]-dependent lifetime. In the presence of 300 μM of TCEP (Figure 4b, orange and Figure 4c) an almost complete disassembly of structures after 16 h was observed, while the same effect could be reached in less than 4 h at a higher concentration of TCEP (3 mM; Figure 4b, red and Figure 4c). Statistical analysis of the microscopy images confirmed the modulation of the transient assembly achieved at different concentrations of reducing agent (Supporting Information, Figure S12).

To demonstrate the versatility of this approach, we have designed a strategy to achieve control over the transient disassembly of DNA-based nanostructures. Also, the design of this system was based on the same nanotube-producing DNA tiles. To demonstrate redox control over the transient disassembly of DNA nanotubes, we have designed a DNA inhibitor strand that by binding to one of the sticky ends of the tile causes the disassembly of the structure. The inhibitor sequence was split into two halves linked by a disulfide bond (Figure 5). Upon reduction of such a disulfide, the two halves will spontaneously de-hybridize from the tiles leading to the re-assembly of the structure over time (Figure 5).

To demonstrate this new strategy, we have tested nanotube disassembly using a set of disulfide inhibitors of different lengths in the presence of a reducing agent (Figure 6a, see Figure S13 in the Supporting Information for schemes of the reaction). Also in this case shorter inhibitors (Inhib_6 and Inhib_10) did not lead to tiles' inactivation and nanotube structures remained stable after addition of the inhibitors (Figure 6b–d). On the other hand, longer inhibitors (Inhib_22 and Inhib_26) allow tile inactivation and consequent nanotube disassembly. However, no re-assembly was observed even after a long time (namely, 24 h) likely because the reduction of the disulfide bond for these inhibitors does not lead to the de-hybridization of the two reduced fragments

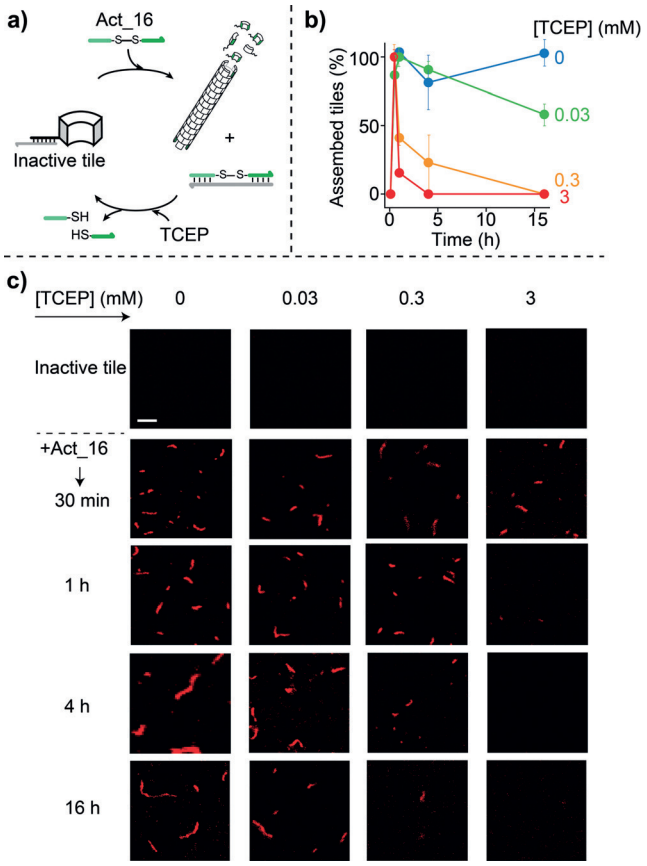

Figure 4. Modulation of the transient self-assembly of DNA-based nanostructures. a) Transient self-assembly induced by a disulfide activator can be modulated by varying the concentration of the reducing agent (TCEP). b) Normalized assembled tile density (assembled tile count/mm^2 for nanotubes longer than 1 μm) measured from the fluorescence microscopy images obtained before and after (30 min, 6 h, 16 h, and 24 h) the addition of the disulfide activator (Act_16) in the presence of different concentrations of TCEP. The experiments shown in this Figure were performed in 1×TAE, 12.5 mM $MgCl_2$ at pH 8.0, 25 °C with different concentration of TCEP (indicated in the Figure). Nanotube self-assembly was carried out in the presence of inactive DNA tiles (500 nM) by adding the disulfide or the control activators (3 μM). The experimental values represent averages of three separate measurements and the error bars reflect the standard deviations. Scale bars for all microscopy images, 2.5 μm.

from the tiles. Only the disulfide inhibitors with intermediate lengths (Inhib_14 and Inhib_18) showed transient disassembly with no nanotubes observed after 1 h from inhibitor addition and micron-scales structures observed upon full reduction of the inhibitor (after 24 h; Figure 6b–d and Supporting Information, Figure S14). Of note, also in this case, the control experiment using inhibitors of the same length, but lacking the disulfide bond showed that nanotubes efficiently disassemble with inhibitors longer than 10 nucleotides after 1 h and do not reform over the 24 h duration of the experiment (Figure 6c and Supporting Information, Figure S15). As an example, microscopy images for the 14-nt control disulfide are shown (Figure 6d, Ctrl). Gel electrophoresis experiments further confirmed that the disulfide inhibitor (Inhib_14) efficiently binds to the DNA tile and de-

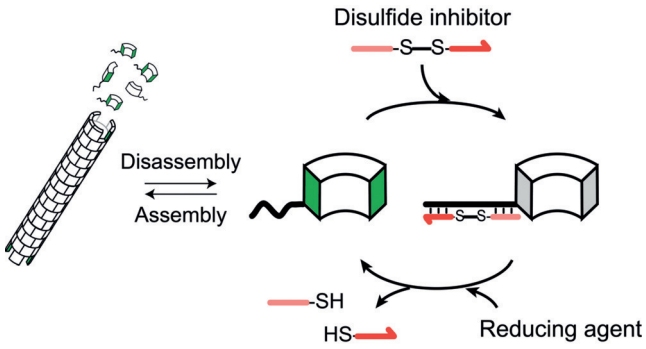

Figure 5. Transient disassembly of DNA-based nanostructures driven by redox fuels. A disulfide inhibitor (red) binds to one of the sticky ends of the tile and drives the transition of the DNA tiles from the active (green tile) to the inactive form (grey tile). This triggers the disassembly of the tubular DNA structures. In the presence of a reducing agent, the disulfide inhibitor is split into its two halves that spontaneously de-hybridize from the tiles making them able to self-assemble again.

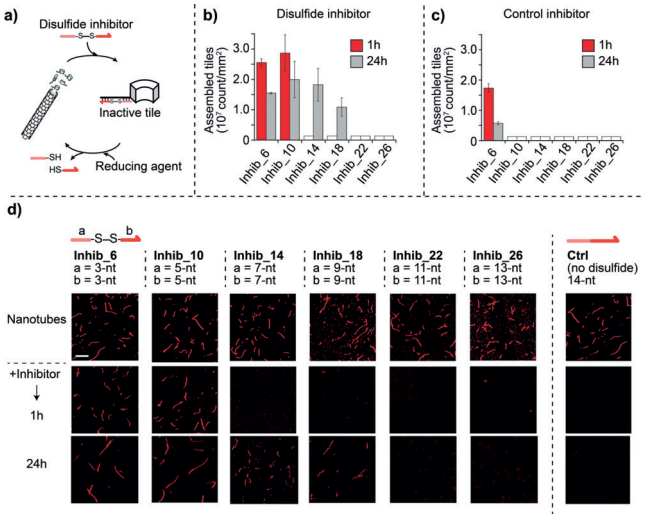

Figure 6. Transient disassembly of DNA-based nanostructures driven by redox fuels. a) Transient disassembly induced by a disulfide inhibitor achieved in the presence of a reducing agent. b) Histograms of assembled tile density (assembled tile count/mm^2) measured from fluorescence microscopy images taken before and after (1 h and 24 h) the addition of disulfide inhibitors of different lengths. c) Same experiment as in (a) but using control inhibitors lacking the disulfide bond. d) Fluorescence microscopy images obtained with the disulfide inhibitors and one control inhibitor (Ctrl_14). The number associated to each inhibitor's name indicates its total number of nucleotides. In (d) the number of nucleotides of the two halves is also indicated. The experiments shown in this Figure were performed in 1×TAE, 12.5 mM $MgCl_2$ at pH 8.0 + TCEP (0.1 mM), 25 °C. Nanotube disassembly was carried out in the presence of nanotubes formed from active DNA tiles (500 nM) by adding the disulfide or the control inhibitor (1 μM). In the histograms (b,c) the bars corresponding to "Assembled tiles" = 0 where no nanotubes are observed are shown as white bars for a matter of clarity. The experimental values represent averages of three separate measurements and the error bars reflect the standard deviations. Scale bars for all microscopy images, 5 μm.

hybridizes upon reduction while shorter (6-nt) and longer (26-nt) inhibitors did not show any transient behaviour (Supporting Information, Figure S16).

Also for this strategy the transient behaviour of nanotube disassembly can be modulated by varying the concentration of the reducing agent (namely, TCEP) employed during the disassembly experiment (Figure 7) as also confirmed by statistical analysis of the microscopy images (Supporting Information, Figure S17). We note here that while we used a disulfide inhibitor longer than the disulfide activator used for transient activation experiments (Figure 4), the rate of transient disassembly (Figure 7b) is slower than that of transient assembly (Figure 4b). This difference is likely due to the difference in kinetics between assembly and disassembly processes with the latter one being much faster.

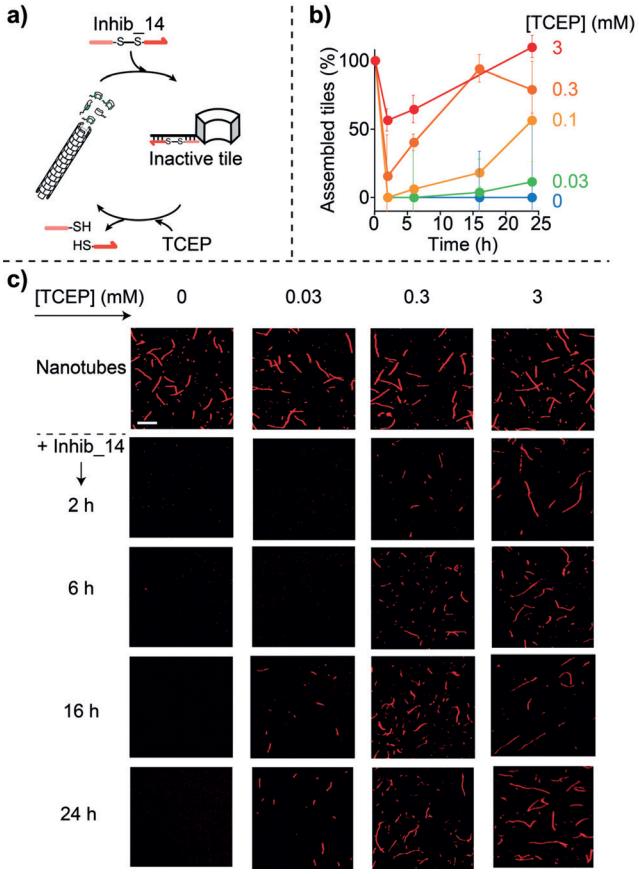

Figure 7. Modulation of the transient disassembly of DNA-based nanostructures. a) Transient disassembly induced by a disulfide inhibitor can be modulated by varying the concentration of the reducing agent (TCEP). b) Normalized assembled tile density (assembled tile count/mm^2, for nanotubes longer than 1 μm) measured from the fluorescence microscopy images obtained before and after (2, 6, 16, and 24 h) the addition of the disulfide inhibitor (Inhib_14) in the presence of different concentrations of TCEP. The experiments shown in this Figure were performed in 1×TAE, 12.5 mM $MgCl_2$ at pH 8.0, 25 °C with different concentration of TCEP (indicated in the Figure). Nanotube disassembly was carried out in the presence of nanotubes formed from active DNA tiles (500 nM) by adding the disulfide or the control inhibitor (1 μM). The experimental values represent averages of three separate measurements and the error bars reflect the standard deviations. Scale bars for all microscopy images, 5 μm.

The redox control over DNA assembly/disassembly demonstrated here offers the possibility to kinetically regulate in an orthogonal way different nanostructures. To demonstrate this, we have employed in the same solution two different DNA nanostructures each assembled by tiles formed by a different set of DNA strands and labelled with two different fluorophores (Q570 and Q670) to permit discrimination by fluorescence imaging. The disassembly of each nanostructure can be specifically addressed by a DNA inhibitor strand with a specific sequence which is selective for the respective DNA nanostructure. Both DNA nanotubes were successfully assembled in the same solution (Figure 8a, left, and 8b) and we initially added the disulfide inhibitor specific for one of the two nanostructures and observed its transient disassembly while the other nanostructure remained stable over the entire duration of the experiment (Figure 8a, Inhibitor #1). Once the re-assembly of the first nanostructure was completed (upon reduction of the first inhibitor), we added the disulfide inhibitor specific for the second nanostructure. The transient disassembly of only the second nanostructure was observed while the size and length of the first nanostructure did not change (Figure 8a, Inhibitor #2).

Both strategies we have described above are fully reversible and multiple cycles can be performed. To demonstrate this, we first tested cyclic additions of the disulfide inhibitor to demonstrate reversible transient disassembly of the DNA structures. More specifically, after the first addition of the disulfide inhibitor we waited for the complete re-assembly of nanotubes observed upon completion of the reduction reaction and we then added a new aliquot of the disulfide inhibitor to the same solution. We observed the same transient behaviour with regrowth of nanotubes of length and number similar to those observed before the addition (Figure 9a). A third cycle of transient disassembly showed the same reversible behaviour. A similar trend was also observed by cyclic additions of the disulfide activator to demonstrate reversibility in the transient self-assembly of the DNA nanotubes (Supporting Information, Figure S18). In a different experiment we have demonstrated reversibility by adding to the same solution, after the completion of the reduction reaction, an oxidizing agent (namely, H_2O_2) to recreate the oxidized disulfide inhibitor. Also in this case, we could observe efficient reversibility over 2 cycles of reduction/oxidation of the transient disassembly (Figure 9b).

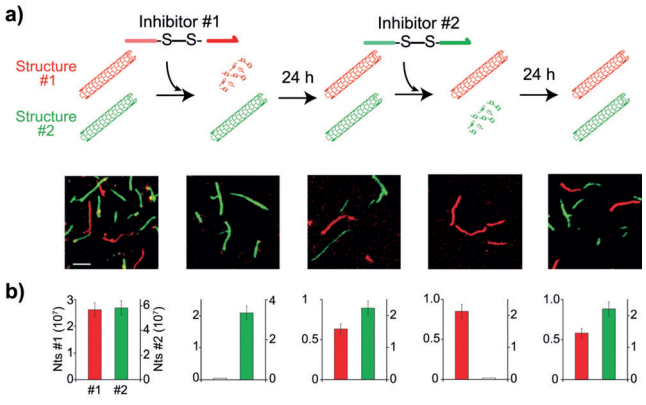

Figure 8. Orthogonal transient disassembly of DNA-based nanostructures driven by redox fuels. a) Two different nanostructures each labelled with a different fluorophore were used here. Each nanostructure can be disassembled by a specific disulfide inhibitor. The addition of the disulfide inhibitor specific for one of the two nanostructures causes the transient disassembly only of one nanostructure while the other remains assembled. b) Histograms of assembled tile density (assembled tile count/mm^2) measured from fluorescence microscopy images. The experiments shown in this Figure were performed in 1×TAE, 12.5 mM $MgCl_2$ at pH 8.0 + TCEP (0.15 mM), 25 °C. Nanotube disassembly was carried out in the presence of both nanotubes formed from active DNA tiles (500 nM) by adding the specific disulfide inhibitor (2 μM). Experimental values represent averages of three separate measurements and the error bars reflect the standard deviations. Scale bars for all microscopy images, 2.5 μm.

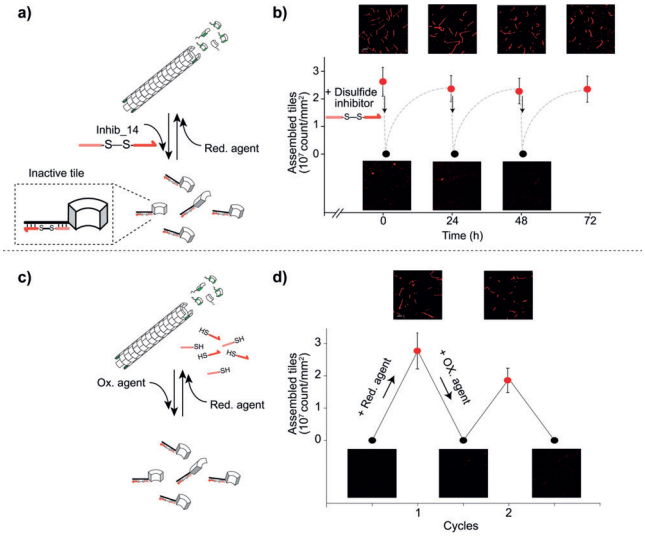

Figure 9. Reversible transient disassembly of DNA-based nanostructures driven by redox fuels. a) After each transient disassembly cycle a new addition of the disulfide inhibitor was performed to demonstrate reversibility. b) Similarly, the inhibitor can be cyclically reformed through the oxidation of the two split reduced thiols in solution by adding an oxidizing agent after each transient disassembly cycle. The experiments shown in this Figure were performed in 1×TAE, 12.5 mM $MgCl_2$ at pH 8.0 + TCEP (0.5 mM), 25 °C. In both experiments the nanotube disassembly was carried out in the presence of nanotubes formed from active DNA tiles (500 nM) by adding the disulfide inhibitor (1 μM). In (a) after each transient cycle (24 h) a new aliquot of the disulfide inhibitor was added (1 μM). In (b) after the transient disassembly cycle (24 h) an oxidizing agent (i.e. H_2O_2, 1 mM) was added to reform the inhibitor. In the following cycles saturating concentrations of TCEP (2 mM) and H_2O_2 (3 mM) were cyclically added. The experimental values represent averages of three separate measurements and the error bars reflect the standard deviations. Scale bars for all microscopy images, 5 μm.

Conclusion

Herein, we have reported a strategy to kinetically control the self-assembly and disassembly of DNA nanostructures using redox reactions. The approach we propose here is versatile and, in contrast to the examples reported to date for the dissipative self-assembly of DNA-based structures,[44,45] does not involve the use of any biomolecular machinery

(enzymes, transcription biomachinery, amongst others). This resembles what happens in Nature where dissipative control is not only achieved with enzymes recognizing and catalysing the hydrolysis of small molecule fuels (ATP, GTP, amongst others), but also through thiol-disulfide redox reactions that can activate or inhibit sulfur switches acting as biological sensors.[49,51] Different subcellular compartments, for example, present different redox potential that allow such redox sensors to be independently maintained under non-equilibrium dynamic control. Inspired by these examples, our strategy demonstrates an alternative approach to control, in a purely synthetic chemical way, the dissipative assembly and disassembly of DNA-based nanostructures.

Similar examples have been also reported for the synthesis of dissipative supramolecular assemblies driven by chemical-reaction cycles,[21,23,55] including redox reactions.[55–61] In our case, the versatility of DNA-based assembly and the predictability of the involved interactions offer the possibility to kinetically control both assembly and disassembly of the nanostructures and to finely control their lifetime in a way that would be difficult to achieve with other synthetic approaches. Our strategy is in fact solely based on redox cycles of reduction/oxidation of disulfide DNA strands acting as regulators for the assembly or disassembly of DNA-based tubular structures that, once reduced, loose their regulation functionality and allow the system to return to its native resting state. The same approach could be conveniently employed to more complex DNA origami[62,63] or to achieve transient structural reconfiguration of DNA structures.[39] As redox oscillations in cells control many biochemical pathways it would also be of great interest to show similar behaviour in synthetic DNA systems.[64,65] Finally, a similar strategy could also be applied to achieve dissipative control of DNA-based nanodevices and might represent an important advancement towards the kinetic control of DNA-based reactions.

Acknowledgements

This work was supported by Associazione Italiana per la Ricerca sul Cancro, AIRC (project n. 21965) (FR), by the European Research Council, ERC (Consolidator Grant project n. 819160) (FR). We thank Elena Romano, Department of Biology, University of Rome Tor Vergata, for support in the confocal microscopy images.

Conflict of interest

The authors declare no conflict of interest.

Keywords: DNA nanotechnology · DNA structures · nonequilibrium processes · self-assembly · supramolecular chemistry

[1] T. Aida, E. W. Meijer, S. I. Stupp, *Science* **2012**, *335*, 813 – 817.
[2] M. J. Webber, E. A. Appel, E. W. Meijer, R. Langer, *Nat. Mater.* **2016**, *15*, 13 – 26.
[3] T. F. De Greef, M. M. Smulders, M. Wolffs, A. P. Schenning, R. P. Sijbesma, E. W. Meijer, *Chem. Rev.* **2009**, *109*, 5687 – 5754.
[4] X. Yan, F. Wang, B. Zheng, F. Huang, *Chem. Soc. Rev.* **2012**, *41*, 6042 – 6065.
[5] D. B. Amabilino, D. K. Smith, J. W. Steed, *Chem. Soc. Rev.* **2017**, *46*, 2404 – 2420.
[6] O. Ikkala, G. Ten Brinke, *Science* **2002**, *295*, 2407 – 2409.
[7] H.-A. Klok, S. Lecommandoux, *Adv. Mater.* **2001**, *13*, 1217 – 1229.
[8] U. Feldkamp, C. M. Niemeyer, *Angew. Chem. Int. Ed.* **2006**, *45*, 1856 – 1876; *Angew. Chem.* **2006**, *118*, 1888 – 1910.
[9] E. Busseron, Y. Ruff, E. Moulin, N. Giuseppone, *Nanoscale* **2013**, *5*, 7098 – 7140.
[10] S. Yagai, A. Kitamura, *Chem. Soc. Rev.* **2008**, *37*, 1520 – 1529.
[11] N. Roy, B. Bruchmann, J.-M. Lehn, *Chem. Soc. Rev.* **2015**, *44*, 3786 – 3807.
[12] L. J. Prins, D. N. Reinhoudt, P. Timmerman, *Angew. Chem. Int. Ed.* **2001**, *40*, 2382 – 2426; *Angew. Chem.* **2001**, *113*, 2446 – 2492.
[13] X. Ma, H. Tian, *Acc. Chem. Res.* **2014**, *47*, 1971 – 1981.
[14] A. Desai, T. J. Mitchison, *Annu. Rev. Cell Dev. Biol.* **1997**, *13*, 83 – 117.
[15] H. Hess, J. L. Ross, *Chem. Soc. Rev.* **2017**, *46*, 5570 – 5587.
[16] D. R. W. Hodgson, M. Schröder, *Chem. Soc. Rev.* **2011**, *40*, 1211 – 1223.
[17] R. Merindol, A. Walther, *Chem. Soc. Rev.* **2017**, *46*, 5588 – 5619.
[18] S. A. P. Van Rossum, M. Tena-Solsona, J. H. Van Esch, R. Eelkema, J. Boekhoven, *Chem. Soc. Rev.* **2017**, *46*, 5519 – 5535.
[19] F. Della Sala, S. Neri, S. Maiti, J. L. Chen, L. J. Prins, *Curr. Opin. Biotechnol.* **2017**, *46*, 27 – 33.
[20] S. Maiti, I. Fortunati, C. Ferrante, P. Scrimin, L. J. Prins, *Nat. Chem.* **2016**, *8*, 725 – 731.
[21] J. Boekhoven, W. E. Hendriksen, G. J. M. Koper, R. Eelkema, J. H. Van Esch, *Science* **2015**, *349*, 1075 – 1079.
[22] J. Boekhoven, A. M. Brizard, K. N. K. Kowlgi, G. J. M. Koper, R. Eelkema, J. H. Van Esch, *Angew. Chem. Int. Ed.* **2010**, *49*, 4825 – 4828; *Angew. Chem.* **2010**, *122*, 4935 – 4938.
[23] B. Rieß, R. K. Grötsch, J. Boekhoven, *Chem* **2020**, 6, 552 – 578.
[24] A. Sorrenti, J. Leira-Iglesias, A. Sato, T. M. Hermans, *Nat. Commun.* **2017**, *8*, 15899.
[25] S. Dhiman, A. Jain, M. Kumar, S. J. George, *J. Am. Chem. Soc.* **2017**, *139*, 16568 – 16575.
[26] A. Mishra, D. B. Korlepara, M. Kumar, A. Jain, N. Jonnalagadda, K. K. Bejagam, S. Balasubramanian, S. J. George, *Nat. Commun.* **2018**, *9*, 1295.
[27] F. Zhang, J. Nangreave, Y. Liu, H. Yan, *J. Am. Chem. Soc.* **2014**, *136*, 11198 – 11211.
[28] N. C. Seeman, H. F. Sleiman, *Nat. Rev. Mater.* **2017**, *3*, 17068.
[29] P. W. K. Rothemund, *Nature* **2006**, *440*, 297 – 302.
[30] H. Ramezani, H. Dietz, *Nat. Rev. Genet.* **2020**, *21*, 5 – 26.
[31] P. Chidchob, H. F. Sleiman, *Curr. Opin. Chem. Biol.* **2018**, *46*, 63 – 70.
[32] K. E. Bujold, et al., *Chem. Sci.* **2014**, *5*, 2449 – 2455.
[33] a) P. Chidchob, D. Offenbartl-Stiegert, D. McCarthy, X. Luo, J. Li, S. Howorka, H. F. Sleiman, *J. Am. Chem. Soc.* **2019**, *141*, 1100 – 1108; b) A. Heuer-Jungemann, T. Liedl, *Trends Chem.* **2019**, *1*, 799 – 814.
[34] W. C. Liao, C. H. Lu, R. Hartmann, F. Wang, Y. S. Sohn, W. J. Parak, I. Willner, *ACS Nano* **2015**, *9*, 9078 – 9086.
[35] H. Ijäs, S. Nummelin, B. Shen, M. A. Kostiainen, V. Linko, *Int. J. Mol. Sci.* **2018**, *19*, 2114.
[36] W. U. Dittmer, A. Reuter, F. C. Simmel, *Angew. Chem. Int. Ed.* **2004**, *43*, 3550 – 3553; *Angew. Chem.* **2004**, *116*, 3634 – 3637.
[37] E. J. Cho, J. W. Lee, A. D. Ellington, *Annu. Rev. Anal. Chem.* **2009**, *2*, 241 – 264.
[38] V. A. Turek, R. Chikkaraddy, S. Cormier, B. Stockham, T. Ding, U. F. Keyser, J. J. Baumberg, *Adv. Funct. Mater.* **2018**, *28*, 1706410.

[39] T. Gerling, K. F. Wagenbauer, A. M. Neuner, H. Dietz, *Science* **2015**, *347*, 1446 – 1452.
[40] D. Gateau, A. Desrosiers, A. Vallée-Bélisle, *Nano Lett.* **2016**, *16*, 3976 – 3981.
[41] A. Kuzyk, M. Urban, A. Idili, F. Ricci, N. Liu, *Sci. Adv.* **2017**, *3*, e1602803.
[42] Q. Jiang, Q. Liu, Y. Shi, Z. G. Wang, P. Zhan, J. Liu, C. Liu, H. Wang, X. Shi, L. Zhang, J. Sun, B. Ding, M. Liu, *Nano Lett.* **2017**, *17*, 7125 – 7130.
[43] Y. Hu, A. Cecconello, A. Idili, F. Ricci, I. Willner, *Angew. Chem. Int. Ed.* **2017**, *56*, 15210 – 15233; *Angew. Chem.* **2017**, *129*, 15410 – 15434.
[44] L. N. Green, H. K. K. Subramanian, V. Mardanlou, J. Kim, R. F. Hariadi, E. Franco, *Nat. Chem.* **2019**, *11*, 510 – 520.
[45] S. Agarwal, E. Franco, *J. Am. Chem. Soc.* **2019**, *141*, 7831 – 7841.
[46] E. Del Grosso, A. Amodio, G. Ragazzon, L. J. Prins, F. Ricci, *Angew. Chem. Int. Ed.* **2018**, *57*, 10489 – 10493; *Angew. Chem.* **2018**, *130*, 10649 – 10653.
[47] J. Deng, A. Walther, *J. Am. Chem. Soc.* **2020**, 142, 2, 685 – 689.
[48] L. Heinen, A. Walther, *Sci. Adv.* **2019**, *5*, eaaw0590.
[49] D. Hamdane, L. Kiger, S. Dewilde, B. N. Green, A. Pesce, J. Uzan, T. Burmester, T. Hankeln, M. Bolognesi, L. Moens, M. C. Marden, *J. Biol. Chem.* **2003**, *278*, 51713 – 51721.
[50] C. Klomsiri, P. A. Karplus, L. B. Poole, *Antioxid. Redox Signaling* **2011**, *14*, 1065 – 1077.
[51] M. Kemp, Y. M. Go, D. P. Jones, *Free Radical Biol. Med.* **2008**, *44*, 921 – 937.
[52] P. W. Rothemund, A. Ekani-Nkodo, N. Papadakis, A. Kumar, D. K. Fygenson, E. Winfree, *J. Am. Chem. Soc.* **2004**, *126*, 16344 – 16352.
[53] D. Y. Zhang, R. F. Hariadi, H. M. T. Choi, E. Winfree, *Nat. Commun.* **2013**, *4*, 1965.
[54] E. Del Grosso, A. Idili, A. Porchetta, F. Ricci, *Nanoscale* **2016**, *8*, 18057 – 18061.
[55] J. Leira-Iglesias, A. Sorrenti, A. Sato, P. A. Dunne, T. M. Hermans, *Chem. Commun.* **2016**, *52*, 9009 – 9012.
[56] S. M. Morrow, I. Colomer, S. P. Fletcher, *Nat. Commun.* **2019**, *10*, 1011.
[57] J. Leira-Iglesias, A. Tassoni, T. Adachi, M. Stich, T. M. Hermans, *Nat. Nanotechnol.* **2018**, *13*, 1021.
[58] J. P. Wojciechowski, A. D. Martin, P. Thordarson, *J. Am. Chem. Soc.* **2018**, *140*, 2869 – 2874.
[59] D. Spitzer, L. L. Rodrigues, D. Straßburger, M. Mezger, P. Besenius, *Angew. Chem. Int. Ed.* **2017**, *56*, 15461 – 15465; *Angew. Chem.* **2017**, *129*, 15664 – 15669.
[60] K. Jalani, S. Dhiman, A. Jain, S. J. George, *Chem. Sci.* **2017**, *8*, 6030 – 6036.
[61] S. Dhiman, R. Ghosh, S. J. George, *ChemSystemsChem* **2019**, *1*, e1900042.
[62] S. Woo, P. W. Rothemund, *Nat. Chem.* **2011**, *3*, 620 – 627.
[63] Z. Zhao, Y. Liu, H. Yan, *Nano Lett.* **2011**, *11*, 2997 – 3002.
[64] J. S. O'Neill, A. B. Reddy, *Nature* **2011**, *469*, 498 – 503.
[65] J. Rutter, M. Reick, L. C. Wu, S. L. McKnight, *Science* **2001**, *293*, 510 – 514.

Manuscript received: February 11, 2020
Revised manuscript received: April 15, 2020
Accepted manuscript online: April 27, 2020
Version of record online: July 9, 2020

